IEEE Access
Multidisciplinary ⋮ Rapid Review ⋮ Open Access Journal

Received 15 August 2024, accepted 4 September 2024, date of publication 10 September 2024,
date of current version 19 September 2024.

Digital Object Identifier 10.1109/ACCESS.2024.3457546

RESEARCH ARTICLE

The Remaining Capacity Estimation of Li-Ion Battery Based on Regional Ultrasonic Energy Characteristic

ZHIDUAN CAI[1,2], (Member, IEEE), HAOYE JIANG[3], LIHAO XU[1,2], AND CHENWEI QIN[3]
[1]School of Intelligent Manufacturing, Huzhou College, Huzhou 313000, China
[2]Huzhou Key Laboratory of Green Energy Materials and Battery Cascade Utilization, School of Intelligent Manufacturing, Huzhou College, Huzhou 313000, China
[3]School of Engineering, Huzhou University, Huzhou 313000, China

Corresponding author: Lihao Xu (xulihao@zjhzu.edu.cn)

This work was supported in part by the Basic Public Welfare Research Program of Huzhou under Grant 2022gz02.

ABSTRACT In recent years, the application of ultrasonic detection technology in the estimation of lithium battery performance states has achieved some results, such as remaining capacity. The remaining capacity is characterized by using ultrasonic feature quantities under a certain state of charge. Such methods to extract features can lead to a phenomenon that multiple ultrasonic signals may correspond to a single state of charge, increasing the contingency of feature extraction and reducing the accuracy of remaining capacity estimation. To this end, an ultrasonic regional energy characterization method is proposed in this paper to enhance the accuracy, and the correlation between ultrasonic regional energy feature quantity and remaining capacity is analyzed. Then the intervals and sampling points to select feature quantities are decided, and the least squares method is utilized to build the capacity degradation model, which can estimate remaining capacity. Finally, the feasibility and effectiveness of the proposed estimation method are verified through experiments.

INDEX TERMS Lithium power battery, ultrasonic detection, regional energy feature, least squares, remaining capacity.

I. INTRODUCTION

With the advantages of high energy density, low self discharge rate and long service life, lithium power batteries have been extensively applied to new energy vehicles, consumer electronics, aerospace and aeronautics [1]. As a kind of energy carrier [2], the remaining capacity of Li-ion battery is one of the key parameters, which directly affects the stability, reliability, and safety [3]. Due to the complicated electrochemical processes and the uncertainty of operating conditions, the degradation mechanism is complex, which makes the estimation of remaining capacity difficult [4]. Accordingly, the estimation with accuracy and rapidity is of great significance, and it is the main focus of battery health management.

The associate editor coordinating the review of this manuscript and approving it for publication was Geng-Ming Jiang.

Ultrasonic detection is widely used with the principle that the propagation speed of ultrasound varies in different media. Ultrasound has been applied to detect the state of batteries [5], [6], [7], [8], [9], [10], [11]. The state characterization of battery is the process of extracting acoustic features from ultrasonic response signals to characterize battery states such as State Of Charge (SOC) and State Of Health (SOH), while acoustic features mainly include amplitude, flight time, sound attenuation coefficient, guided wave signal, etc.

Studies [8], [9], [10] extract the above features from ultrasonic response signals and their correlations with SOC, whose prediction models are established combined with machine-learning. The work reveals that the change of acoustic signal is caused by the change of internal materials, and the relation is explained by acoustic modeling. The possibility of estimating SOC through acoustic methods is proved. Yi et al. [11] discover the time of flight (ToF) and signal amplitude (SA) of ultrasound is closely related

to the charge-discharge cycles and aging degree. Further research indicates that ToF and SA can be utilized to estimate remaining capacity as well as establishing SOH estimation model.

The above results are based on the ultrasonic features under the corresponding single SOC state respectively, while multiple SOC states are ignored. Due to the step-wise change trend of SOC during charging-discharging cycles, a SOC corresponds not to a single time point, but to a time period, while ultrasonic response signals are collected at regular intervals, which leads to a single SOC responding to multiple response signals within the corresponding time period. Therefore, the contingency of feature characterization is increased and estimation accuracy is reduced. To this end, an regional feature quantity (FQ) characterisation method to characterize remaining capacity is proposed, relevant FQs based on regional data are extracted, and the selection of intervals and sampling points is optimised. Then, the least squares method are applied to establish a lithium battery degradation model, which describes the relationship between the proposed FQs and remaining capacity. Finally the model performance is verified through experiments, which is proved to be a new method for the estimation of the remaining capacity of lithium batteries.

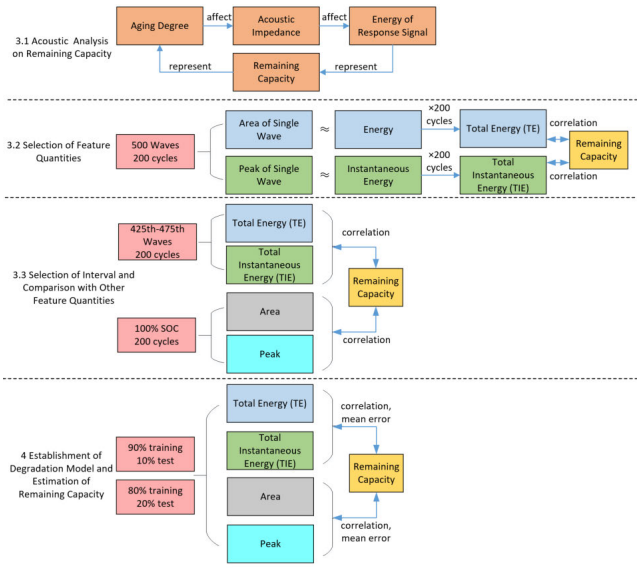

FIGURE 1. The process of the proposed estimating methods.

The experiment platform to conduct ultrasonic detection is introduced in Section II. The mapping relationship between response signal and remaining capacity is analyzed in section III-A. The selection of feature quantities is proceeded in section III-B. Further, the appropriate intervals of feature quantities are selected and the comparison with other feature quantities is developed in section III-C. The establishment of degradation model and the estimation of remaining capacity is conducted in section IV. The work in this article is summarized in section V. The overall estimation process is illustrated in Fig.1:

II. EXPERIMENT PLATFORM

As represented in Fig.2, the remaining capacity detection device for Li-ion battery consists of a Xinwei BTS cycle charging-discharging device, a thermostat, and an ultrasonic detection module (MITCCH MUT550B, 100KHz). The ultrasonic transmitting and receiving probes are respectively placed at the center of the upper and the corresponding lower surfaces of the battery to be tested, fixed with coupling agent and fixing device, as depicted in Fig.3. The receiving probe is connected to a PC, which runs a data acquisition program in MATLAB to save and display the waveform data of response signal.

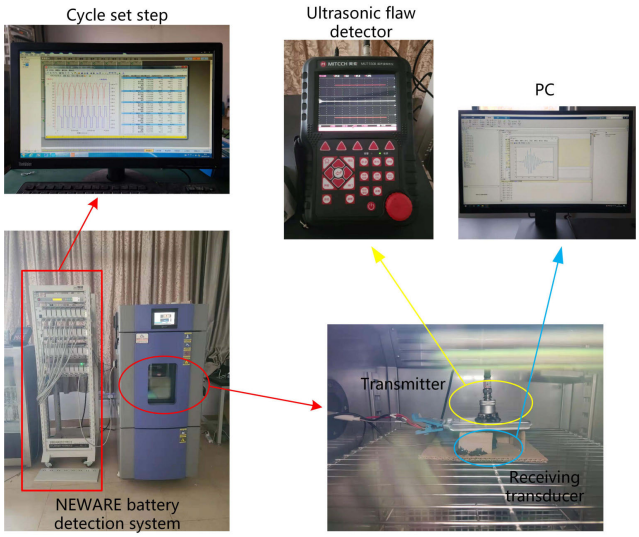

FIGURE 2. Detection device.

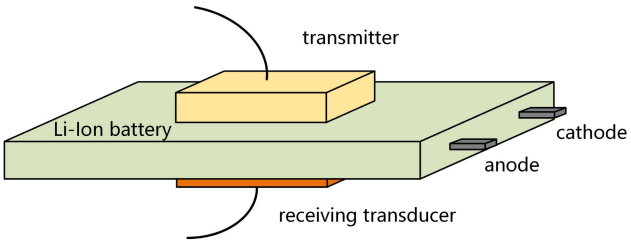

FIGURE 3. The position of probes and batteries.

During experiment, a 10000 mAH soft-pack lithium battery was placed in the thermostat, and the battery was cycled using the charge-discharge instrument. The parameters for the settings are displayed in Table 1.

Ultrasonic signal pulses are generated every 5s, after penetrating the lithium battery, the receiving probe transmits the received response signal to the PC for data saving.

III. DATA ANALYSIS AND FEATURE EXTRACTION

During the charging-discharging cycles, the insertion/ extraction of Li-ions may cause variable volume of the

TABLE 1. Battery parameters and experimental conditions.

	Constant current charge	Constant voltage charge	Shelve	Constant current discharge
Current(mA)	6000(0.6C)	cutoff 20	-	6000(0.6C)
Voltage(V)	cutoff 4.2	4.2	-	cutoff 2.7
Time(min)	-	-	10	-

negative electrode active material, which will lead to the cracking of the negative solid electrolyte interface (SEI), exposing the active material to the electrolyte again, forming a new SEI film. The addition of SEI film results in the relaxation of the lattice structure, increasing the Young's modulus of material, and causes battery aging with reduced capacity. The aging of lithium batteries is accompanied by lithium deposition, electrode material relaxation, and other phenomena, all of which can lead to changes in the Young's modulus and density of the electrode material. Therefore, the remaining capacity of lithium batteries is directly related to the properties above. Besides, due to the sensitivity of ultrasound to the properties, an electrochemical-acoustic coupling relationship can be established, as in (1):

$$Z_{ultra} = \sqrt{\rho E} \tag{1}$$

where Z_{ultra}, ρ and E represent acoustic impedance, material density and Young's modulus respectively. It is revealed in equation that the density and Young's modulus determine the magnitude of the acoustic impedance, which affects the attenuation of energy when the ultrasound penetrates the medium, and results in the variance of response signal energy. Due to the multi-layered and heterogeneous nature of lithium-ion batteries [5], there is no well-established model to describe the specific relationship between acoustic impedance and attenuation [11]. However, it is known that the amplitude and energy of ultrasound are influenced by impedance and are closely related to material density and Young's modulus. According to the analysis above, the remaining capacity of batteries can be characterized by ultrasonic responding signals for its correlation with the amplitude and energy of ultrasound.

A. SELECTION OF THE FEATURE QUANTITIES OF TOTAL ENERGY

Fig.4 displays an ultrasonic response signal in a sampling window, with the horizontal axis representing the sampling window and the vertical axis representing the signal amplitude. The sampling window size is 12 us. Through experiments, it is found that by subdividing 12 us into 1200 sampling time points, a complete response signal can be received. Owing to the long duration of a single charge-discharge cycle, in a certain cycle, there are also many ultrasonic response signals under a fixed sampling window.

Fig.5 depicts the ultrasonic response signals with different cycle times under the same sampling window. It can be concluded that as the number of cycles increases, the battery gradually ages, the amplitude of the response signal decreases, so does the area enclosed by the signal and the horizontal axis (the area of ultrasonic response signal). Fig.5 indicates that the loss of ultrasonic with the same energy is different when penetrating lithium batteries with different degrees of aging.

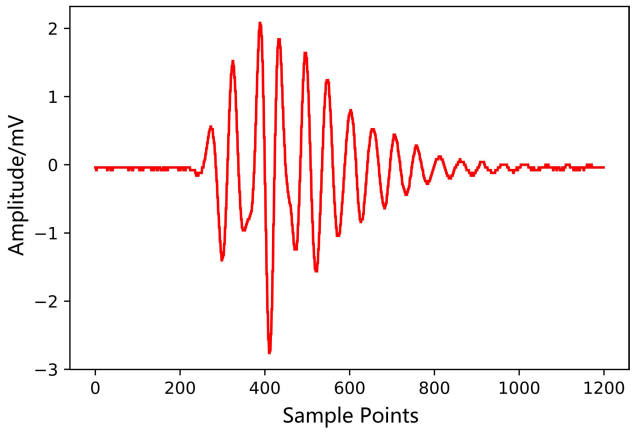

FIGURE 4. Ultrasonic response signal.

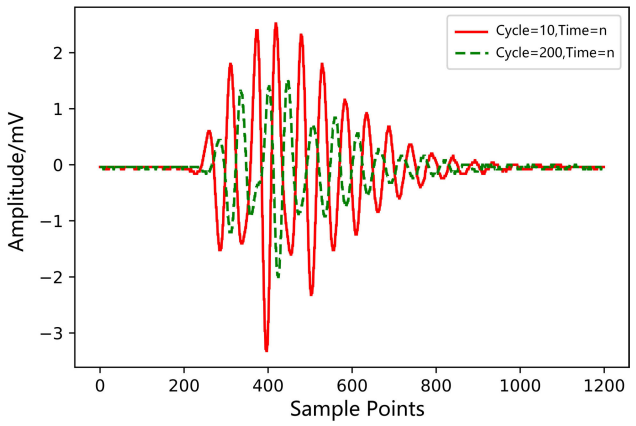

FIGURE 5. Comparison of ultrasonic response signals at the same discharge moment in different cycles.

The ultrasonic energy loss is defined in (2), where $P_{receive}$, P_{pulse} and $P_{attenuation}$ are the energy received by probe, generated by probe, and attenuated during penetration, respectively. The more serious the battery aging is, the greater the energy loss during transmission, the smaller the received energy by probe, and the smaller the response signal area. Therefore, the ultrasonic response area can be used to characterize the remaining capacity at current number of cycles, as shown in the blue part of Fig.6.

$$P_{\text{receive}} = P_{\text{pulse}} - P_{\text{attenuation}} \tag{2}$$

As the aging of batteries intensifies, the time for a single charge-discharge cycle under the same conditions reduces. Since ultrasonic sampling is done at a fixed time, this results in different number of sampling windows under different

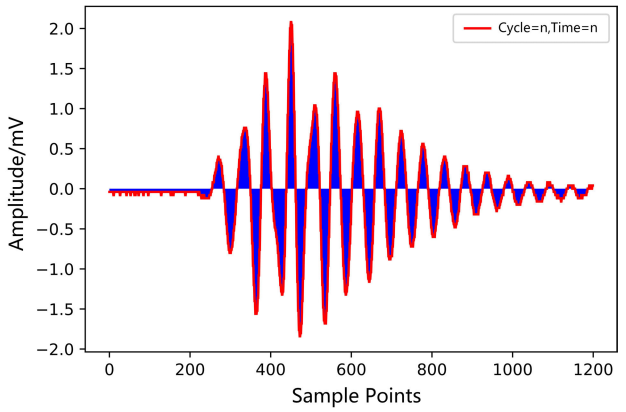

FIGURE 6. The enclosed area of response signal.

cycle times. As shown in Fig.7, it is a graph of the relationship between cycles times and sampling windows numbers. It is visible in the graph that as the number of cycles increases, the aging becomes more severe, the charging-discharging time decreases, and so does the number of sampling windows per cycle. In order to ensure that there are the same number of sampling windows in all cycles, the maximum common number is taken. By analysing, the paper sets the number of sampling windows in a single cycle to 500, with a sampling interval of 5 s, resulting in a total sampling time of 2500 s, approximately.

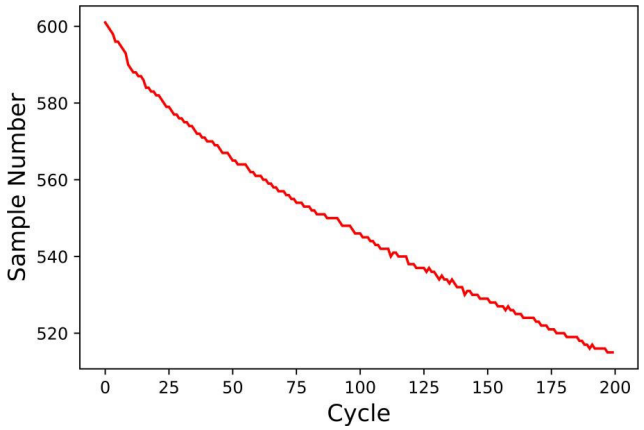

FIGURE 7. The number of sampling windows under different cycle times.

The area of 500 sampled response waveforms in a single cycle is calculated, that is, the ultrasonic energy feature under current sample window, and 500 energy features as trend curves are plotted. Similarly, the same calculation method is also applied to batteries with different cycle times, after the energy feature extraction of ultrasonic response signal, the results as shown in Fig.8. The horizontal axis is the number of sample windows of response signals in a single cycle, and the vertical axis is the calculated FQ. As shown in Fig.8, with the discharge process continues, the SOC decreases, and the energy FQ also decreases accordingly. As the number of cycles increases, the energy FQ of ultrasonic response signals are significantly different under different cycle times, and the overall trend remains downward.

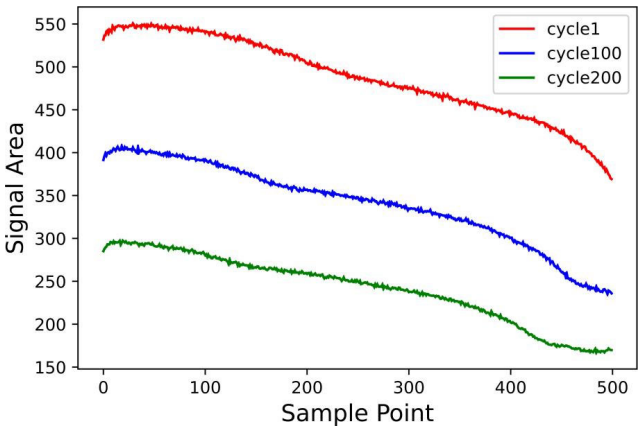

FIGURE 8. The area of sampled waveforms under different charge-discharge cycles.

As illustrated in Fig.8, there are 500 FQs in a single cycle. In order to characterize the remaining capacity using a single FQ, the area enclosed by the curve and the horizontal axis in Fig.8 (total energy FQ) is used to characterize the remaining capacity in the current cycle, as depicted in the yellow portion of Fig.9. The yellow part can be regarded as the total energy FQ of the response signal in a single cycle. Similar total energy FQ calculation was performed on other charge-discharge cycles, and the results are depicted in Fig.10. The horizontal axis represents the number of cycles, and the vertical axis represents the total energy of the ultrasonic signal. As shown in Fig.10, as the number of cycles increases, the remaining capacity decreases, and the total energy FQ of the ultrasonic signal also shows a downward trend.

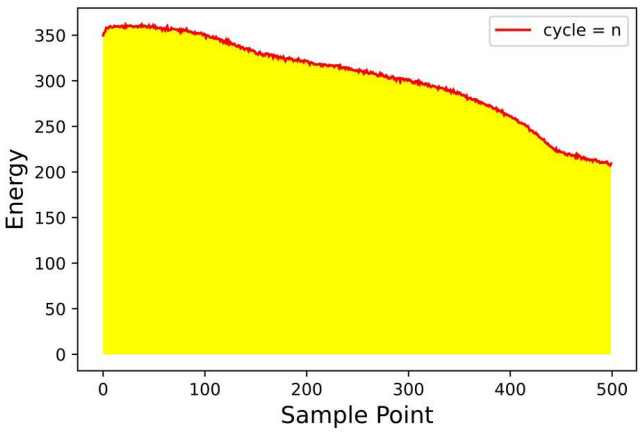

FIGURE 9. Total energy of the response signal in a single cycle.

In order to investigate the correlation between the ultrasonic signal FQ and the remaining capacity of the battery, a quantitative analysis was carried out using the Pearson

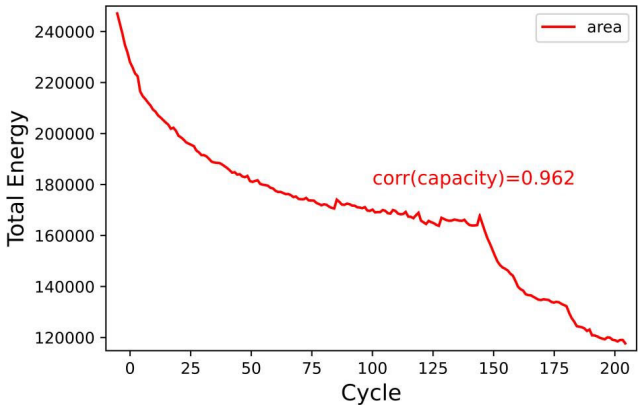

FIGURE 10. The total energy under different cycles.

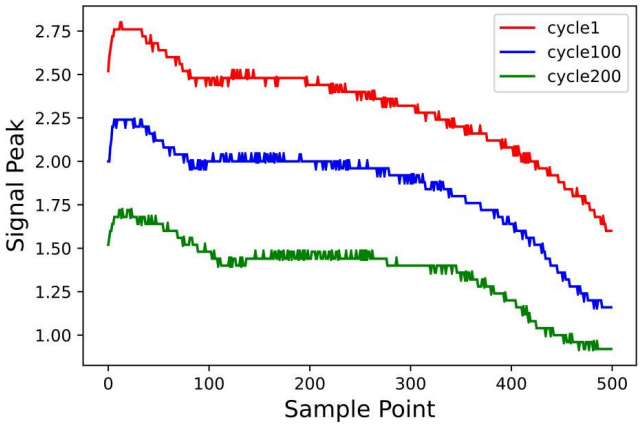

FIGURE 11. The peak of sampled waveforms under different charge-discharge cycles.

correlation coefficient analysis method. As shown in (3), x and y are correlation quantities, x_i and y_i are the *ith* samples of correlation quantities, $\overline{x}$ and $\overline{y}$ are sample means:

$$corr_{x,y} = \frac{\Sigma(x-\overline{x})(y-\overline{y})}{(\sqrt{\sum_{i=1}^{n}(x_i-\overline{x})^2})(\sqrt{\sum_{i=1}^{n}(y_i-\overline{y})^2})} \quad (3)$$

The $corr()$ function value in Fig.10 is the Pearson correlation coefficient between the total energy of the ultrasonic signal and the remaining capacity. From this value (0.962), it can be judged that the total energy of the ultrasonic signal is strongly correlated with the remaining capacity.

B. SELECTION OF THE FEATURE QUANTITIES OF TOTAL INSTANTANEOUS ENERGY

It can be revealed in Fig.5 that in addition to the enclosed area, the response signals at different cycle times have distinct differences in peak values, which represent the maximum instantaneous energy. Similar to the area feature extraction method, 500 maximum instantaneous energy FQs are selected in a single cycle, as shown in Fig.11. The curves in Fig.11 display the trend of maximum instantaneous energy FQs in different cycles. It can be seen from the figure that the maximum instantaneous energy FQs in a single cycle gradually decreases as the discharge process continues. As the number of cycles increases, the remaining capacity and the amplitude of the curves gradually decrease.

Similarly, there are 500 peak FQs in a single cycle. In order to characterize the remaining capacity using a single FQ, the area enclosed by the peak FQ curve and the horizontal axis under a single cycle is used to characterize the remaining capacity, as depicted in the orange portion of Fig.12.

The orange part can be regarded as the sum of maximum instantaneous energy of response signal received in a single cycle. Using the same method to characterize other cycles, the results can be gathered in Fig.13. There is a obvious trend in the figure that as the battery degrades, the sum of the maximum instantaneous energy received in a single cycle appears a gradual decrease trend. $corr()$ function in Fig.12 is the calculated value of Pearson correlation coefficient, and

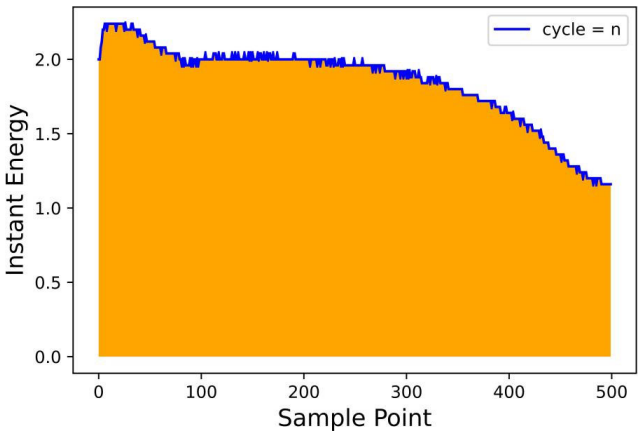

FIGURE 12. Total instantaneous energy of the response signal in a single cycle.

the result implies that the extracted FQ of total instantaneous energy is closely linked to remaining capacity.

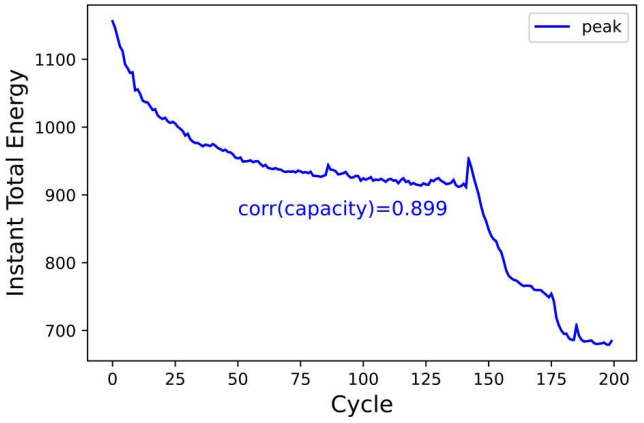

FIGURE 13. The total instantaneous energy under different cycles.

C. SELECTION OF FEATURE QUANTITIES

The above mentioned (the total energy and total instantaneous energy, referred to as TE and TIE respectively) two regional FQs are based on full cycle data, which requires long

intervals, long sampling time and large database. In order to improve the representation ability and extraction efficiency, different sampling intervals and times will be compared in this section to select FQ extraction intervals and sampling points.

To investigate the influence of different sampling intervals on the representation of TEFQ, 500 sampling points in a single cycle were averaged into groups of 100 points each, and the TEFQ as well as the correlation coefficient of each group is calculated to study the remaining capacity representation ability. Fig.14 is a graph of correlation analysis results for different sampling intervals, with the horizontal axis representing average interval, as indicated by *Marker*1 in Table 2, and the vertical axis represents correlation coefficient. In Fig.14, it is evident that after grouping, the FQ based on the sampling points ranging from 400 to 500 has the strongest representation ability.

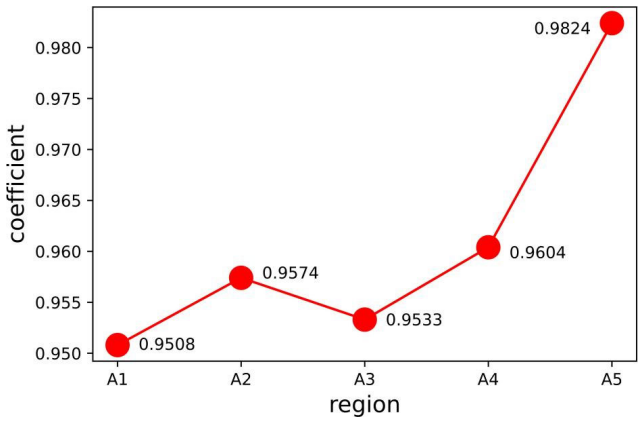

FIGURE 14. The correlation coefficients of TE under mean divided sampling intervals.

TABLE 2. The sampling interval settings of TE.

Marker1	Interval	Marker2	Interval
A1	0-100	A51	400-500, interval, 2
A2	100-200	A52	400-500, interval, 4
A3	200-300	A53	400-500, interval, 5
A4	300-400	A54	400-500, interval, 10
A5	400-500	A55	400-450
		A56	425-475
		A57	450-500

As for different sampling points on the characterisation of TEFQ, the chosen sampling interval from Fig.15 was further disassembled according to the settings in Table 2, *Marker*2, to select suitable number of sampling points. Fig.15 presents the results of different sampling points, in which the horizontal axis represents different points selection methods and the vertical axis represents correlation coefficients. The first four sampling methods are selected at intervals of 2, 4, 5, and 10 within the range of 400 to 500 and the correlation coefficient of TEFQ is calculated. As a result, the number of sampling points corresponding to each TEFQ is 50, 25, 20, and 10, respectively, rather than 500. This approach reduces computational complexity and enhances sampling speed; the latter three methods are conducted in 50 sampling points each and the correlation of TEFQ is also calculated.

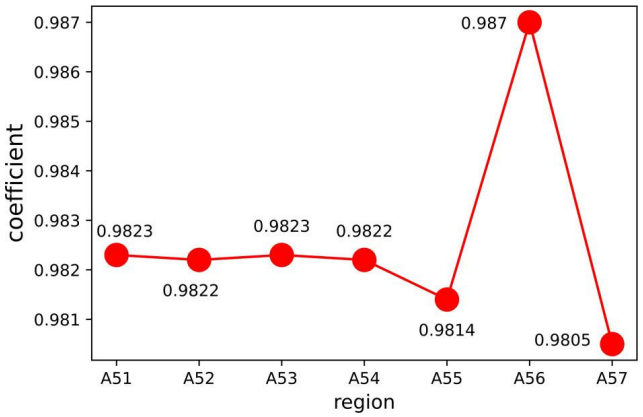

FIGURE 15. The correlation coefficients of TE under non-mean sampling intervals.

Based on Fig.15, it is evident that the TEFQ within 425 to 475 exhibits the best representation ability. Consequently, this study adopts the TEFQ within this interval for subsequent modeling of remaining capacity estimation. In comparison to the original 500 points, the new interval is compressed to 50 points, which not only reduces the data volume but also enhances the correlation.

The optimization method for TIEFQ is similar to that for TE. The settings of sampling intervals and points are as shown in Table 3, and the correlation results are presented in Fig.16 and Fig.17.

TABLE 3. The sampling interval settings of TIE.

Marker1	Interval	Marker2	Interval
B1	0-100	B51	400-500, interval, 2
B2	100-200	B52	400-500, interval, 4
B3	200-300	B53	400-500, interval, 5
B4	300-400	B54	400-500, interval, 10
B5	400-500	B55	400-450
		B56	425-475
		B57	450-500

Among them, Fig.16 illustrates the correlation analysis results of different sampling intervals. It can be seen from the figure that the FQ extracted from sampling points 400 to 500 has the strongest representation ability. Fig.18 further talks the characterization ability with different number of sampling points within 400 to 500. Based on Fig.17, the TIEFQ within 425 to 475 exhibits the strongest characteristic ability. Therefore, it is selected as the second feature for subsequent estimation.

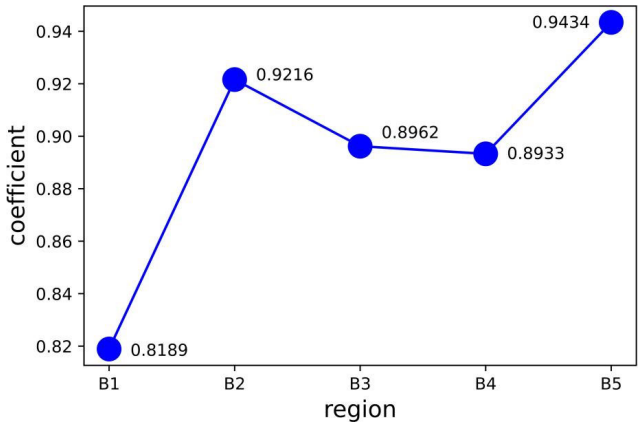

FIGURE 16. The correlation coefficients of TIE under mean divided sampling intervals.

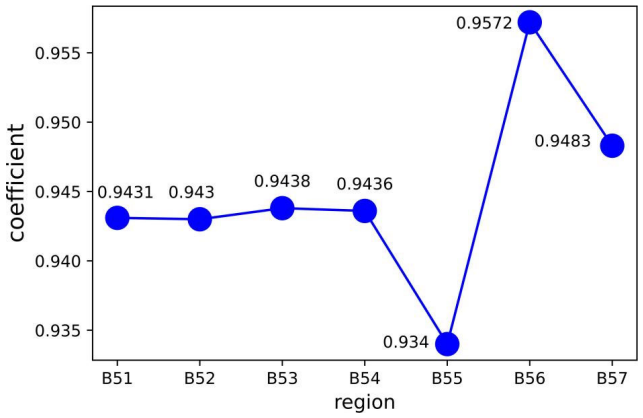

FIGURE 17. The correlation coefficients of TIE under non-mean sampling intervals.

Fig.18 depicts the trend of extracted FQs within the optimized sampling interval. In the figure, *corr*() function is the calculated Pearson correlation coefficient, the horizontal axis is the number of cycles, and the vertical axis is the calculated value of FQ. Compared to Fig.10 and Fig.13, it can be observed that the correlation between the selected FQs and remaining capacity has been obviously enhanced after optimization.

To compare the two FQs proposed above (TEFQ and TIEFQ) and the FQ based on single time point, the area and peak FQs of ultrasonic response signal at SOC = 100% under different cycle numbers are extracted, and the correlation with remaining capacity is calculated, in Fig.19. When the battery is sampled at a single time point, the correlation between the extracted ultrasonic area FQ and the remaining capacity is 0.943, and the correlation between the peak FQ and the remaining capacity is 0.898. Comparing Fig.18 and Fig.19, it can be discovered that the FQ correlation based on regional energy (TE and TIE) is higher than that based on extreme value (area and peak), and the curve is smoother.

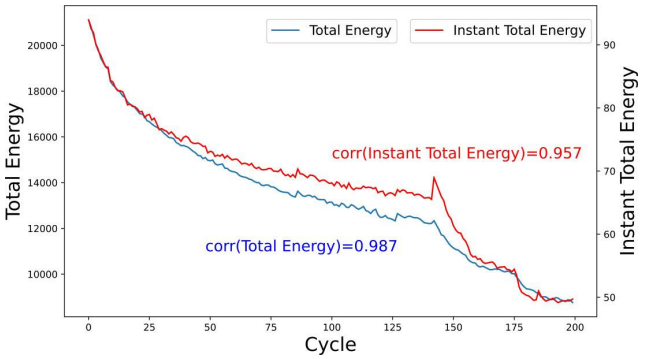

FIGURE 18. The correlation coefficients of TE and TIE under different cycle times.

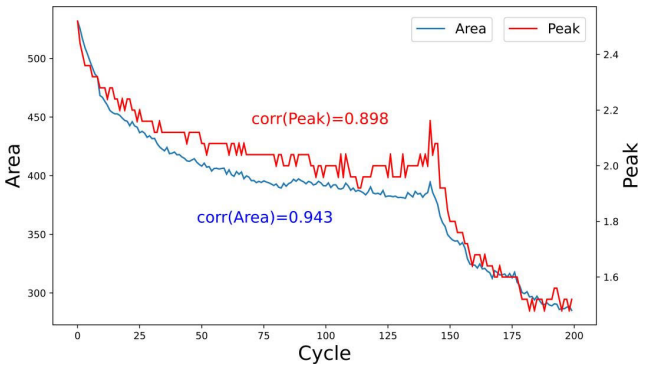

FIGURE 19. The correlation coefficients of area and peak under different cycle times.

IV. ESTABLISHMENT OF CAPACITY DEGRADATION MODEL AND ESTIMATION OF REMAINING CAPACITY

A. ESTABLISHMENT OF CAPACITY DEGRADATION MODEL

The battery capacity degradation model is established based on the extracted TE, TIE FQs, along with the least squares method. The process is illustrated in Fig.20.

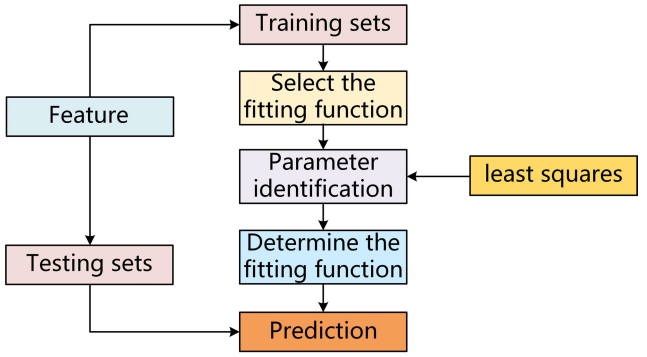

FIGURE 20. The establishment process of battery capacity degradation model.

The dataset, consisting of 200 charge-discharge cycles, is divided into a training set and a testing set. The training set comprises the first 90% of the data, while the testing set

comprises the remaining 10%. The training data is utilized for establishing the degradation model. The testing data is employed to evaluate the performance of the degradation model. To demonstrate the representational capacities of FQs based on single time (area and peak) and interval energy (TE and TIE), this study separately builds capacity degradation models, conducting a comparative analysis.

According to the model construction method described in Fig. 20, the training set sample data is sampled to construct a capacity degradation model based on a single time point FQ, and the model expression is shown in (4).

$$\begin{aligned}\text{Capacity1}_{\text{SOC=1}} &= 4.2902\text{Area}_{\text{SOC=1}} \\ &\quad + 1061.5711\text{Peak}_{\text{SOC=1}} + 5370.6676\end{aligned} \tag{4}$$

where $\text{Capacity1}_{\text{SOC=1}}$ is the predicted output of the degradation model, $\text{Area}_{\text{SOC=1}}$ is area FQ of response signal in a single time point, and $\text{Peak}_{\text{SOC=1}}$ is peak FQ of response signal in a single time point.

Similarly, the capacity degradation model based on regional energy FQ is established, as shown in (5).

$$\begin{aligned}\text{Capacity1}_{\text{Energy}} &= 0.0721\text{Energy}_{\text{Area}} \\ &\quad + 21.777\text{Energy}_{\text{Peak}} + 6686.8224\end{aligned} \tag{5}$$

where $\text{Capacity1}_{\text{Energy}}$ is the predicted output based on energy, while $\text{Energy}_{\text{Area}}$ and $\text{Energy}_{\text{Peak}}$ are TE and TIE FQs respectively.

Based on the training set sample data, two capacity degradation models are applied to calculate the remaining capacity of the battery, and the results are shown in Fig. 21. The blue, red and green curves represent the actual capacity degradation, the capacity calculation result based on single time FQs (area and peak), the capacity calculation result based on regional FQs (TE and TIE) respectively. From the figure, it can be seen that the fitting curves based on regional energy FQs are closer to the actual capacity degradation curve, with higher accuracy.

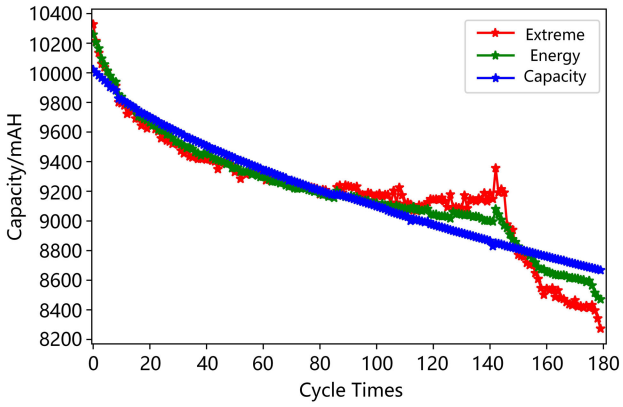

FIGURE 21. The fitting results of degradation model 1.

In order to further investigate the characterisation ability based on regional energy FQs under different prediction starting points, the first 80% of the dataset was used as a training set and the second 20% as a test set for model construction and validation. Equation (6) is a degradation model based on a single time point, and (7) is a degradation model based on regional energy, with individual parameters similar to those in (4) and (5).

$$\begin{aligned}\text{Capacity2}_{\text{SOC=1}} &= 4.8697\text{Area}_{\text{SOC=1}} \\ &\quad + 1347.7089\text{Peak}_{\text{SOC=1}} + 4517.8707\end{aligned} \tag{6}$$

$$\begin{aligned}\text{Capacity2}_{\text{Energy}} &= 0.0744\text{Energy}_{\text{Area}} \\ &\quad + 24.4535\text{Energy}_{\text{Peak}} + 6449.3178\end{aligned} \tag{7}$$

The model fitting is depicted in Fig.22, from which it can be seen that although the training sample data is reduced and the capacity interval to be predicted is increased, the fitting curve based on the regional energy is yet closer to the actual capacity degradation curve and has higher accuracy.

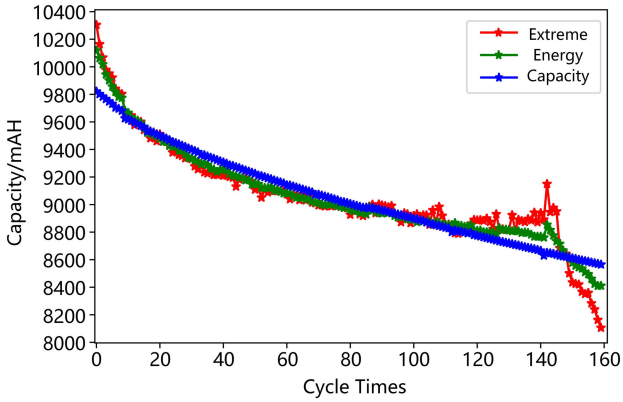

FIGURE 22. The fitting results of degradation model 2.

B. ESTIMATION OF REMAINING CAPACITY

In order to verify the effectiveness of the constructed degradation model for predicting remaining capacity, the latter 10% test set data was substituted into the degradation model ((4) and (5)) to estimate the capacity of the latter 10% batteries, and the results are demonstrated in Fig.23.

The blue curve is the actual capacity degradation curve, the red curve is the prediction result curve of the degradation model based on single time point energy FQ, and the green curve is the prediction result curve based on internal energy FQ. From the experimental results, it can be seen that the degradation model based on internal energy has better prediction performance. The average error is 190 mAH, while that of model based on single time point is 407 mAH. Therefore, the experimental results verify that the estimation performance of model using the internal energy FQs is better than that using single time energy FQs.

Similarly, the latter 20% test data is used to substitute into the degradation models ((6) and (7)) to predict the remaining capacity of the latter 20% batteries, and the results are shown

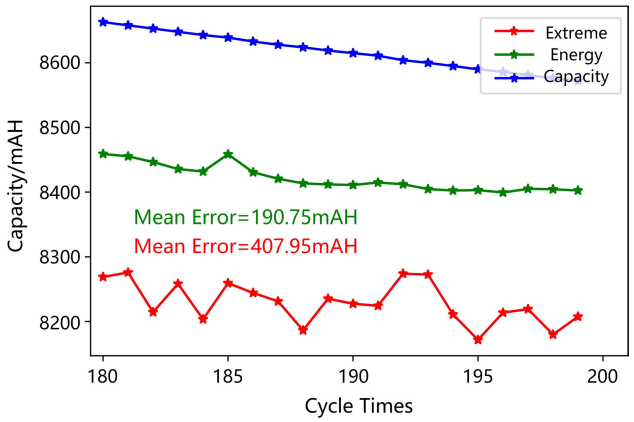

FIGURE 23. Estimation result of degradation model 1.

in Fig.24. The average prediction error of the curve based on single time point energy FQ is 642.63 mAH; the average prediction error of the curve based on the internal energy FQ is 274.76 mAH. From the figure, although the interval need to be estimate is larger, the estimation performance of model using the internal energy FQs is still better and guarantees favourable prediction accuracy.

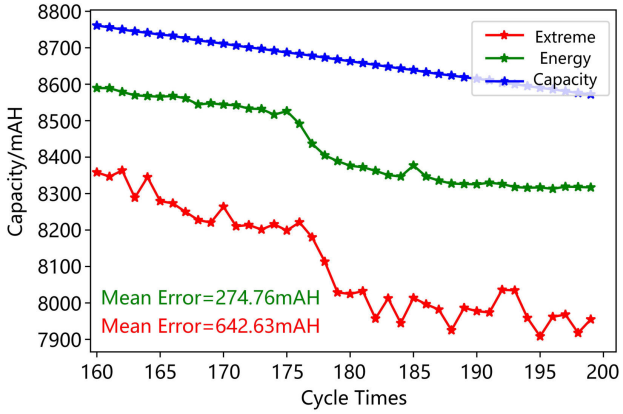

FIGURE 24. Estimation result of degradation model 2.

V. CONCLUSION

Based on the correlation of ultrasonic response signal and capacity degeneration, the FQ of ultrasonic regional energy is proposed to represent the remaining capacity of battery in this paper as well as to enhance the prediction accuracy of remaining capacity. The extraction method of regional energy FQ is studied and analyzed, and the best intervals and numbers of sampling are selected. The least squares method is adopted to fit the relationship model between the regional energy FQ and capacity degradation. The feasibility and effectiveness of the proposed method to estimate the remaining capacity is verified. The paper draws the following conclusions:

(1) Under different charge-discharge cycles of the battery, the collected ultrasonic response signal is correlated with the degradation state of the battery. Based on the response signal, the characteristics such as the area enclosed by the waveform and the horizontal axis (energy feature quantity) can be extracted to characterize the capacity degradation of the battery. In order to ensure that the battery has the same number of ultrasonic sampling windows under different degradation state cycles, the specific sampling period value is given. The above feature extraction method effectively avoids the defect of characterizing the remaining capacity of battery relying on the ultrasonic feature in a single SOC state.

(2) To solve the problem of non-uniqueness caused by multiple energy features generated in a single cycle, two features, TEFQ and TIEFQ, are proposed in this paper. In this way, a single feature is used to characterize the remaining capacity in a certain charge-discharge cycle.

(3) Without reducing the correlation between the extracted FQ and the remaining capacity, localised ultrasonic interval data in a single cycle is used to extract TE and TIE to represent remaining capacity, which enables enhancing extraction speed and reducing computational complexity.

(4) Based on the interval information of the ultrasonic response signal, this paper innovatively extracted two feature quantities, namely, TE and TIE, to characterize the remaining capacity of lithium-ion batteries. It solves the problem of low estimation accuracy caused by using ultrasonic feature under a single SOC in the conventional method. In practical applications such as electric vehicles, lithium-ion power batteries work by building battery packs in series and parallel, and the operating conditions of batteries will also change. Considering variable working conditions and battery pack, further research on the basis of this paper will be carried out.

REFERENCES

[1] X. Gong, R. Xiong, and C. C. Mi, "A data-driven bias-correction-method-based lithium-ion battery modeling approach for electric vehicle applications," *IEEE Trans. Ind. Appl.*, vol. 52, no. 2, pp. 1759–1765, Mar. 2016.

[2] B. Scrosati and J. Garche, "Lithium batteries: Status, prospects and future," *J. Power Sources*, vol. 195, no. 9, pp. 2419–2430, May 2010.

[3] R. Xiong, J. Cao, Q. Yu, H. He, and F. Sun, "Critical review on the battery state of charge estimation methods for electric vehicles," *IEEE Access*, vol. 6, pp. 1832–1843, 2018.

[4] A. V. Virkar, "A model for degradation of electrochemical devices based on linear non-equilibrium thermodynamics and its application to lithium ion batteries," *J. Power Sources*, vol. 196, no. 14, pp. 5970–5984, Jul. 2011.

[5] B. Long, W. Xian, L. Jiang, and Z. Liu, "An improved autoregressive model by particle swarm optimization for prognostics of lithium-ion batteries," *Microelectron. Rel.*, vol. 53, no. 6, pp. 821–831, Jun. 2013.

[6] Z. Cai, H. Jiang, T. Pan, C. Qin, J. Xu, and Y. Wang, "Remaining capacity prediction of li-ion batteries based on ultrasonic signals," *J. Chin. Inst. Engineers*, vol. 47, no. 2, pp. 215–225, Feb. 2024.

[7] Z. Cai, T. Pan, H. Jiang, Z. Li, and Y. Wang, "State-of-charge estimation of lithium-ion batteries based on ultrasonic detection," *J. Energy Storage*, vol. 65, Aug. 2023, Art. no. 107264.

[8] R. Li, W. Li, H. Zhang, Y. Zhou, and W. Tian, "On-line estimation method of lithium-ion battery health status based on PSO-SVM," *Frontiers Energy Res.*, vol. 9, pp. 693249–693261, Jul. 2021.

[9] X. Cui and T. Hu, "State of health diagnosis and remaining useful life prediction for lithium-ion battery based on data model fusion method," *IEEE Access*, vol. 8, pp. 207298–207307, 2020.

[10] P. Kurzweil, W. Scheuerpflug, B. Frenzel, C. Schell, and J. Schottenbauer, "Differential capacity as a tool for SOC and SOH estimation of lithium ion batteries using charge/discharge curves, cyclic voltammetry, impedance spectroscopy, and heat events: A tutorial," *Energies*, vol. 15, no. 13, p. 4520, Jun. 2022.
[11] M. Yi, F. Jiang, L. Lu, S. Hou, J. Ren, X. Han, and L. Huang, "Ultrasonic tomography study of metal defect detection in lithium-ion battery," *Frontiers Energy Res.*, vol. 9, p. 909, Dec. 2021.

ZHIDUAN CAI (Member, IEEE) was born in Jiangxi, China, in 1978. He received the master's degree in mechanical design and theory from Jingdezhen Ceramic University, China, in 2007. His research interests include intelligent manufacturing technology, performance state evaluation, and health management of lithium-ion batteries in electrical vehicles.

HAOYE JIANG was born in Zhejiang, China, in 1997. He received the B.Eng. degree in electrical engineering and automation from Huzhou College, Huzhou, China, in 2020. He is currently pursuing the M.Sc. degree in electronic information with Huzhou University. His current research interests include life estimation and health management of lithium-ion batteries in electrical vehicles.

LIHAO XU was born in Zhejiang, China, in 1996. He received the bachelor's degree in traffic equipment and control from Northwestern Polytechnical University, China, in 2018, and the master's degree in control engineering from Zhejiang University, China, in 2021. His research interests include the control of aerial robots and health management of lithium-ion batteries in electric vehicles.

CHENWEI QIN was born in Zhejiang, China, in 1998. He received the B.Eng. degree in electrical engineering and automation from Huzhou University, Huzhou, China, in 2020. He is currently pursuing the M.Sc. degree in electronic information with Huzhou University. His current research interests include life estimation and health management of lithium-ion batteries in electrical vehicles.